iScience

CellPress
OPEN ACCESS

Article

Inflammation conditional genome editing mediated by the CRISPR-Cas9 system

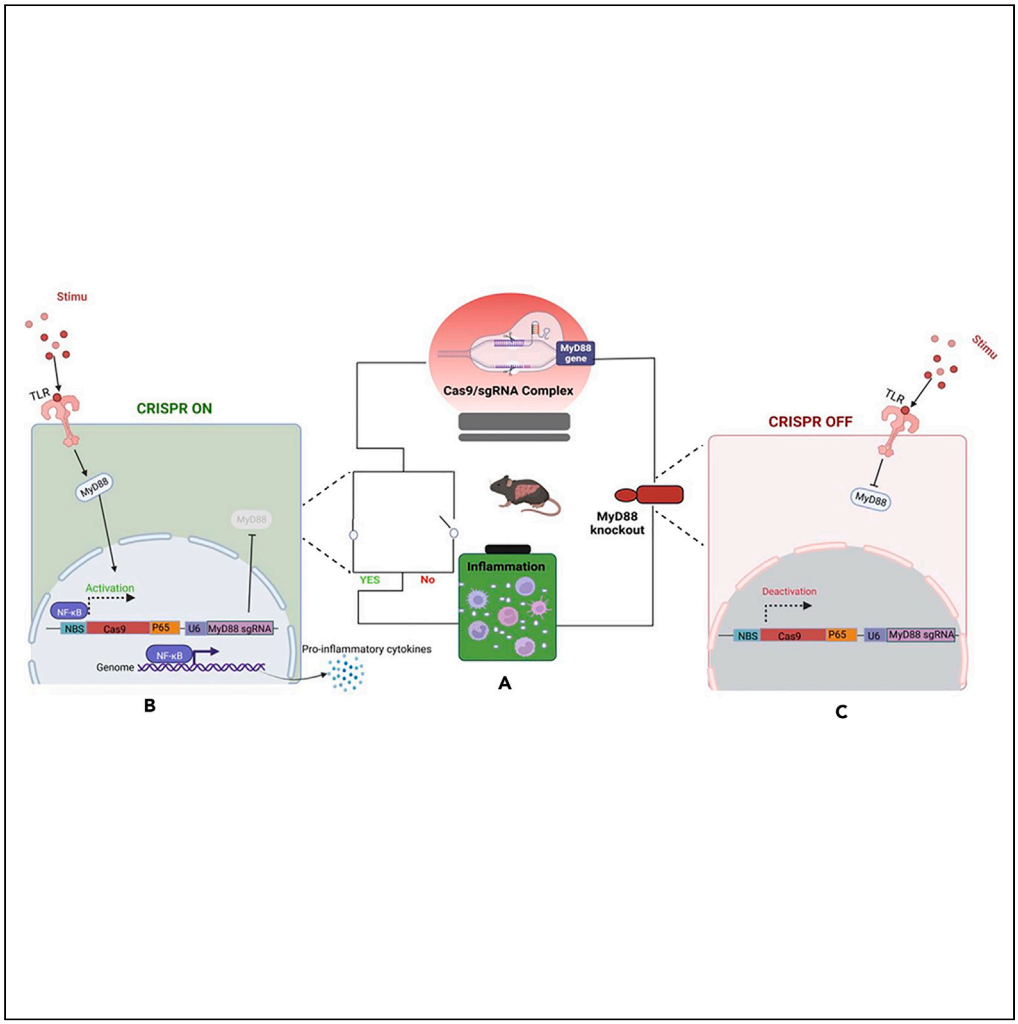

Tingting Yuan, Honglin Tang, Xiaojie Xu, ..., Young-Chang Cho, Yuan Ping, Guang Liang

yccho@chonnam.ac.kr (Y.-C.C.)
pingy@zju.edu.cn (Y.P.)
wzmcliangguang@163.com (G.L.)

Highlights

We developed an inflammation inducible CRISPR/Cas9 system

It limit the gene interrogation to pathological lesion with high editing efficiency

The knockout of MyD88 could switch off this CRISPR/Cas9 circuit

This work provides the insight to CRISPR-based AAV therapeutics

Yuan et al., iScience 26, 106872
June 16, 2023
https://doi.org/10.1016/j.isci.2023.106872

iScience

CellPress
OPEN ACCESS

Article

Inflammation conditional genome editing mediated by the CRISPR-Cas9 system

Tingting Yuan,[1,2,3,5] Honglin Tang,[4] Xiaojie Xu,[2] Jingjing Shao,[1] Gaojun Wu,[1] Young-Chang Cho,[3,*] Yuan Ping,[2,*] and Guang Liang[1,5,6,*]

SUMMARY

The specificity of CRISPR-Cas9 in response to particular pathological stimuli remains largely unexplored. Hence, we designed an inflammation-inducible CRISPR-Cas9 system by grafting a sequence that binds with NF-κB to the CRISPR-Cas9 framework, termed NBS-CRISPR. The genetic scissor function of this developed genome-editing tool is activated on encountering an inflammatory attack and is inactivated or minimized in non-inflammation conditions. Furthermore, we employed this platform to reverse inflammatory conditions by targeting the MyD88 gene, a crucial player in the NF-κB signaling pathway, and achieved impressive therapeutic effects. Finally, during inflammation, P65 (RELA) can translocate to the nucleus from the cytoplasm. Herein, to avoid Cas9 leaky DNA cleavage activity i, we constructed an NBS-P65-CRISPR system expressing the Cas9-p65 fusion protein. Our inflammation inducible Cas9-mediated genome editing strategy provides new perspectives and avenues for pathological gene interrogation.

INTRODUCTION

Inflammation underlies various physical and pathological processes and can be instigated by harmful infections and tissue injuries.[1] Inflammation is generally characterized by the activation and infiltration of immune cells and subsequent release of inflammatory cytokines and chemicals (e.g., tumor necrosis factor-alpha [TNF-α], interleukin [IL]-6, IL-8, leukotrienes prostaglandin, and histamine).[2] There are two types of inflammation, acute and chronic. A considerable inflammatory response can defend the host against infection and restore basal homeostatic conditions. However, sustained inflammation can ultimately lead to irreparable tissue or organ damage—for example, sepsis,[3] gout, cardiovascular disease, diabetes,[4] and Alzheimer's disease.[5] In addition, there is increasing evidence that chronic inflammation is strongly associated with tumorigenesis (e.g., *Helicobacter pylori* infection in gastric cancer, human papillomavirus infection in cervical cancer and hepatitis in liver carcinomas).[6] Various signaling pathways contribute to the onset of inflammation, including the c-Jun N-terminal kinase (JNK) and p38 mitogen-activated protein kinase (p38 MAPK), nuclear factor κ-light-chain-enhancer of activated B cells (NF-κB),[7] TNF, phosphatidylinositol 3-kinase (PI3K), Janus Kinase/Signal Transducers and Activators of Transcription (JAK/STAT), and Hippo pathways. In particular, there is intricate crosstalk between the NF-κB pathway and other signaling pathways. Consequently, this pathway plays a critical role in inflammation, cancer progression, apoptosis, and differentiation.[8] In addition, the cytokine/receptor interactions involved in these pathways are often disrupted in therapeutic strategies targeting inflammation. Therapeutic approaches or pharmacologic interventions in current clinical practice for reducing inflammation include inhibitors, antagonists, blocking antibodies, miRNAs, siRNAs, or shRNAs that can perturb complementary gene expression. Knocking out or knocking down perpetrator genes may produce a better effect than solely disturbing the translation process The CRISPR/Cas9 system is ideal for achieving this goal.

The CRISPR/Cas9 (Clustered Regularly Interspaced Short Palindromic Repeats/CRISPR associated protein 9) system comprises two indispensable modules, (1) Cas9, with endonuclease activity, and (2) an associated single guide RNA (sgRNA) that targets a specific DNA sequence.[9] The potency of the convenient and efficient DNA cleavage achieved with the sgRNA renders CRISPR systems powerful tools for genome engineering in many cells and organisms. CRISPR systems are undergoing continuous optimization; however, there are still some limitations to be addressed regarding their use for gene therapy in clinic. For example, (1) off-target effects, defined as gene interrogation occurring at undesired gene loci, are a matter of concern, (2)

[1]Department of Cardiology, The First Affiliated Hospital of Wenzhou Medical University, Wenzhou, Zhejiang 325035, China

[2]College of Pharmaceutical Sciences, Zhejiang University, Hangzhou, 310058, China

[3]Pharmaceutical Sciences, College of Pharmacy, Chonnam National University, Gwangju, Korea

[4]Department of Medical Oncology, Sir Run Run Shaw Hospital School of Medicine, Zhejiang University, Hangzhou, 310058, China

[5]Chemical Biology Research Center, School of Pharmaceutical Sciences, Wenzhou Medical University, Wenzhou, Zhejiang 325035, China

[6]Lead contact

*Correspondence: yccho@chonnam.ac.kr (Y.-C.C.), pingy@zju.edu.cn (Y.P.), wzmcliangguang@163.com (G.L.)

https://doi.org/10.1016/j.isci.2023.106872

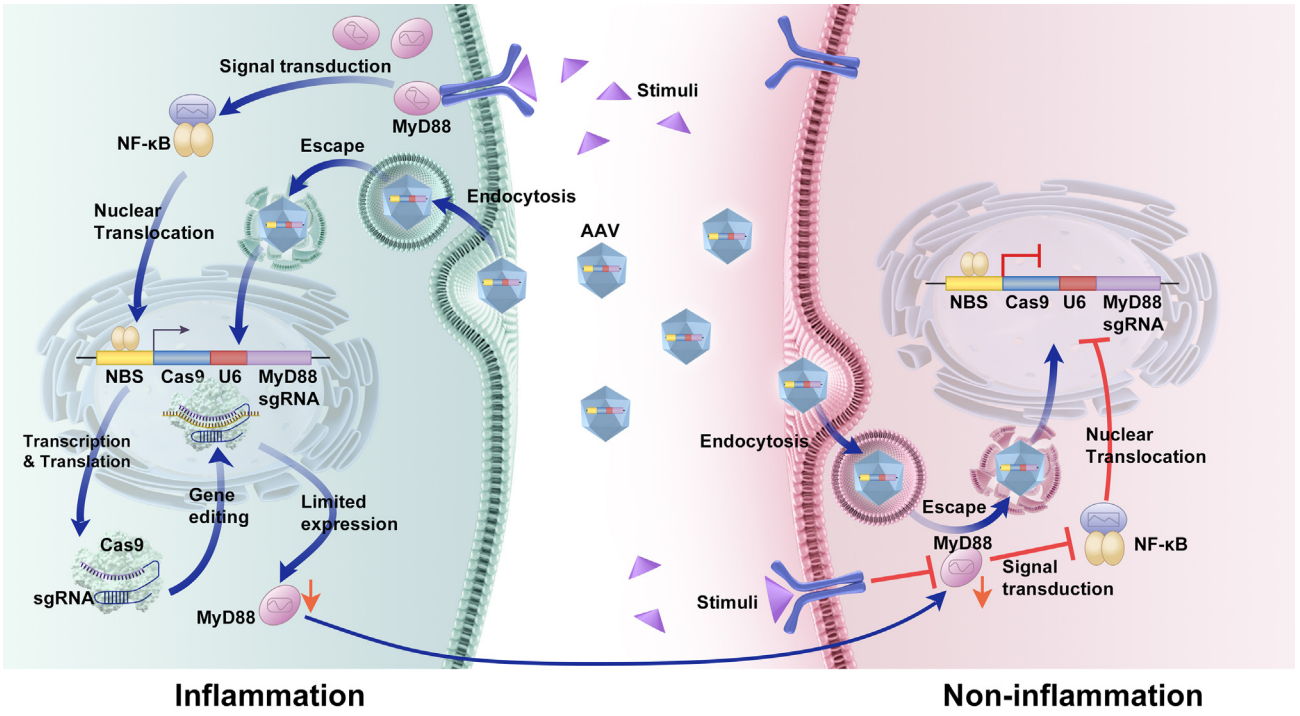

Figure 1. Mechanism of inflammation-induced genome editing mediated by the CRISPR/Cas9 System

A functional CRISPR/Cas9 (termed NBS-CRISPR) plasmid targeting MyD88 was delivered into the nucleus by an AAV9 carrier. External stimuli exposure induced an inflammatory response. The functional CRISPR/Cas9 plasmid translated Cas9 on NF-κB nuclear translocation. MyD88 protein expression was decreased as a result of gene editing. The low expressed MyD88 resulted in the inhibition of the NF-κB pathway on stimulation and alleviated inflammation. Limited NF-κB nuclear translocation switches off the functional CRISPR/Cas9 plasmid.

uncontrollable temporal and spatial DNA cleavage on processes, and (3) low cellular delivery efficiency caused by the large size of the Cas9 transgene system. The challenges described above have promoted continuous innovation regarding this technology, and some orthologous systems have been developed. Feng Zhang and co-workers combined the Cre/*loxP* with the CRISPR/Cas9 system to generate Cre-dependent Cas9 knock-in mice.[10] Then, the same team established an inducible CRISPR/Cas9 system with rapamycin and gained real-time control over genome editing.[11] In the same year, Ortiz et al. developed a split-Cas9 system based on split inteins.[12] Similarly to those, doxycycline- and tamoxifen-inducible CRISPR/Cas9 systems have also been introduced.[13,14] In addition, Ye and co-workers exploited the far-red light-activated split-Cas9 system.[15] The advent of dCas9, based on DNase-inactivated Cas9, has further enriched this system.[16–20] Briefly, these modified dCas9 versions involve fusing the transcription activator (CRISPRa) or repressor (CRISPRi) with dCas9 to enable the manipulation of gene expression by epigenome editing.[21] In parallel with the regulation of Cas9, modifying the sgNRA is also proceeding.[22–26] Such efforts are dedicated to generating a controllable CRISPR/Cas9 system and ultimately decreasing off-target effects. However, apart from the addition of functional CRISPR biocomposites, other exogenous inputs that may disrupt homeostasis must be added. Therefore, in addition to focusing on tissue-specific promoters, another promising avenue is to explore ways the organism itself could act as an inducer of CRISPR systems. Herein, we described here a strategy to limit Cas9 activity in response to inflammation. In contrast to the strategies mentioned above, we grafted the effector of a canonical inflammatory pathway, the NF-κB responsible element, as the promoter of Cas9. When inflammation occurs, NF-κB can translocate to the nucleus and bind with the NF-κB responsible element, thereby activating Cas9 transcription. Furthermore, we knocked out the central node of inflammatory pathway, myeloid differentiation primary response 88 (MyD88). MyD88 is the canonical adaptor that controls the innate immune and inflammation. Myd88 upregulation is associated with inflammation and thus be recognized as a potential drug target.[27] On this basis, impairing Myd88 expression will diminish the inflammatory response, in turn switches off Cas9 transcription (Figure 1). We envision that this strategy will be broadly beneficial to the development of therapies for numerous inflammatory or related disorders mediated by the orthologous CRISPR system.

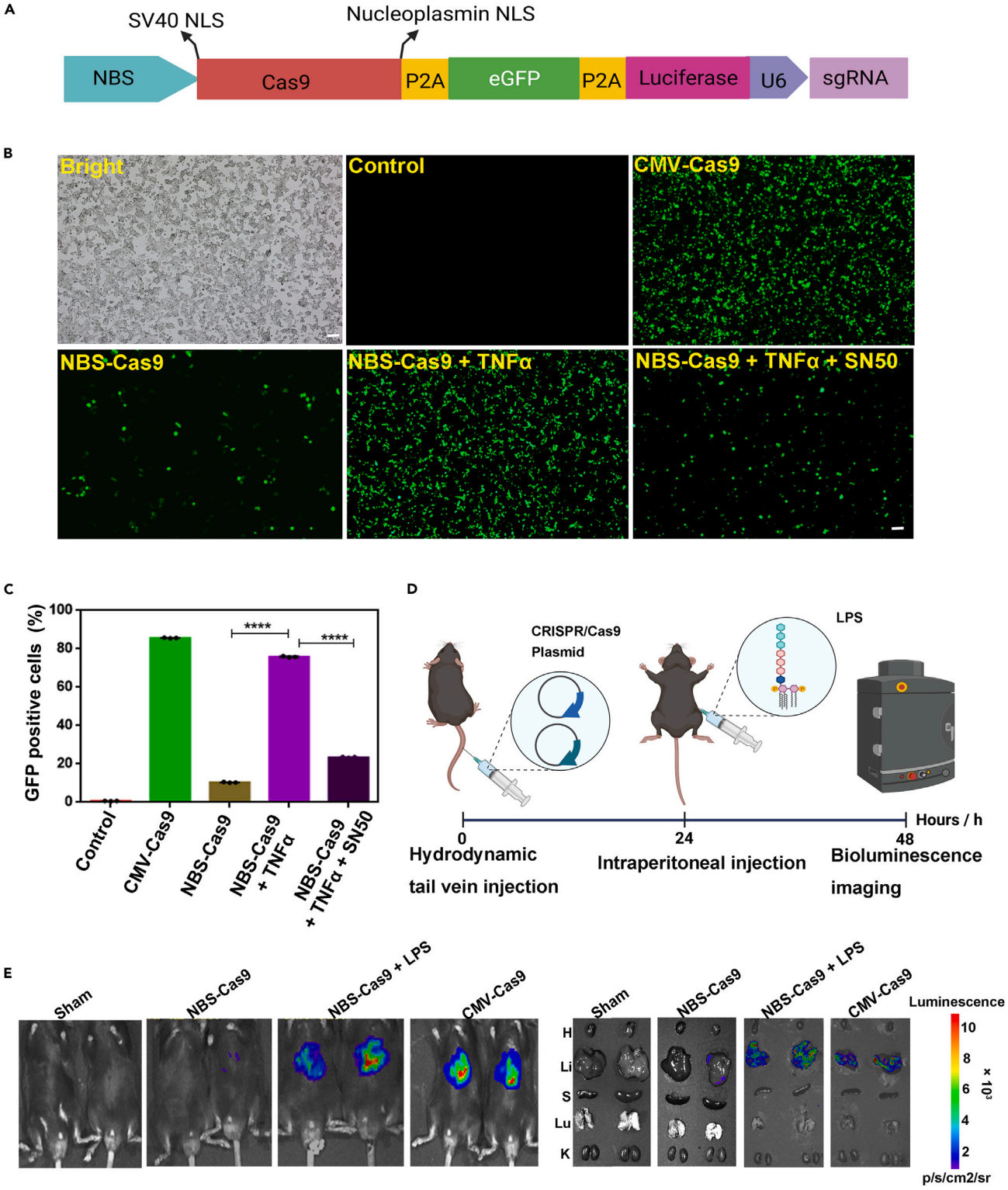

Figure 2. Validation of the concept *in vitro* and *in vivo*

(A) Design of the NBS-CRISPR system. NBS, NF-κB binding sequence.

(B) Transfection and fluorescence microscopy images of HEK293T cells treated with different CRISPR/Cas9 plasmids. Scale bar: 50 μm.

Figure 2. *Continued*

(C) Quantification of GFP-positive cells in the panel (b). Data are presented as the mean ± SEM, n = 3. One-way ANOVA with a Tukey's post-hoc test. ****$p < 0.0001$.

(D) Schematic of the validation of the NBS-Cas9 system *in vivo*.

(E) Detection of luciferase expression after hydrodynamic-based gene delivery in mice (n = 2, left panel) and evaluation of its biodistribution (right panel). H, Heart; Li, Liver; S, Spleen; Lu, Lung; K, Kidney.

RESULTS

Proof-of-concept validation

We sought to insert a promoter upstream of Cas9 to activate Cas9 function under inflammatory conditions. Ultimately, we chose the NF-κB binding sequence (NBS) as the promoter to initiate Cas9 expression (termed NBS-Cas9) because it is well characterized and has established the NF-κB reporter system.[28] Based on the research of Smith EL et al.,[29] we first validated its response to inflammation in a simple framework with mCherry as the reporter in HEK293 cells and the CMV promoter as the positive control (Figure S1). The NBS group demonstrated high reporter expression than the no-simulation group, which was comparable to the CMV group under inflammatory conditions (Figure S2). Furthermore, the effect of NBS can be reversed by the NF-κB inhibitor SN50 (Figure S2). Subsequently, we wondered if the NBS could drive the expression of the larger molecular protein Cas9; thus, we grafted it to the CRISPR/Cas9 framework with enhanced GFP (eGFP) and luciferase as reporters (Figure 2A). Twenty-four hours post-transfection, 50 ng/mL TNF-α was applied to HEK293T cells and incubation for additional 24 h. The results demonstrated that the system functioned robustly when stimulated with TNF-α; however, it could be inhibited when the cells pretreated with SN50 (the NF-κB inhibitor) (Figures 2 B and 2C). Considering that NBS copy number may affect NBS-Cas9 performance, we constructed five NBS-CRISPR plasmids with different NBS copies, NBS1-CRISPR, NBS2-CRISPR, NBS3-CRISPR, NBS5-CRISPR, and NBS7-CRISPR with one, two, three, five, and seven NBS copies, respectively. As the results identified that one or two copies of NBS have almost no effect on Cas9, whereas five copies of NBS had the better performance; thus, NBS5-CRISPR was selected for the subsequent research (Figure S3). Thereafter, we then explored time course of Cas9 induction. We set a timescale of TNF-α stimulation for 24h, 48h, 72h and 96h. As the results showed that with the prolongation of stimulation time, especially after 48 h, the Cas9 protein decreased dramatically (Figure S4). These results align with Sojung Kim et al.'s finding[30] that the Cas9 protein was degraded rapidly in HEK293 T cells 48h after transfection with a lenti-Cas9 plasmid. This effect is potentially related to the degradation of plasmids and Cas9 protein or the dilution of Cas9 protein because of cell proliferation. Finally, to further assess whether this system would perform efficiently *in vivo*, we hydrodynamically injected 20 μg of CRISPR/Cas9 plasmid into C57BL/6 mice. After 24 h, the mice were intraperitoneally injected with LPS (5 mg/kg) to elicit the inflammation response. Bioluminescence imaging was performed 24 h post-LPS stimulation to measure luciferase expression (Figure 2D). Consistent with the *in vitro* results, strong bioluminescence was detected 24 h after LPS stimulation in the NBS-Cas9 group and was more widely enriched in the liver (Figure 2E). These collected data suggested that the concept of the CRISPR/Cas9 system driven by inflammation (or NBS) is practical. The present work also revealed that the plasmid functions mainly in the liver, mediated with a hydrodynamics-based DNA delivery technique, which encouraged us to focus on inflammatory liver failure to evaluate the therapeutic effectiveness of this system.

There are over 20 cell types in the liver; macrophages (or Kupffer cells), which modulate inflammation as gatekeepers,[31] and hepatocytes, which possess multiple complex functions,[32] account for the largest proportions. Consequently, we aimed to examine the responsiveness and therapeutic potential of inflammation-targeting NBS-CRISPR system with MyD88 sgRNA insertion in these two cell types.

NBS-CRISPR system validation in the RAW264.7-cell line

Based on the biological structure of the MyD88 protein,[33] we designed three sgRNAs online (CHOPCHOP [uib.no]) targeting the second, third and fifth exons that separately encode the intermediate domain and Toll-interleukin-1 receptor domain (Figure 3A). Then, we separately integrated these sgRNAs into CRISPR/Cas9 tools promoted by CMV (termed CMV-CRISPR) and transfected them into B16-F10 cells. sgRNA2 was ultimately screened out for subsequent targeting because of its high gene mutation rate (Figure S5). We then cloned sgRNA2 into our functional plasmid and transfected the resulting construct into RAW264.7 cells, followed by stimulation with LPS (1 μg/mL) for 24/48 h to evaluate the initiation of this system and the perturbation of inflammation resulting from MyD88 gene editing (Figure 3B). The results revealed that the rate of GFP-positive cells reached 36% in the NBS-CRISPR plus LPS treated group, close to that

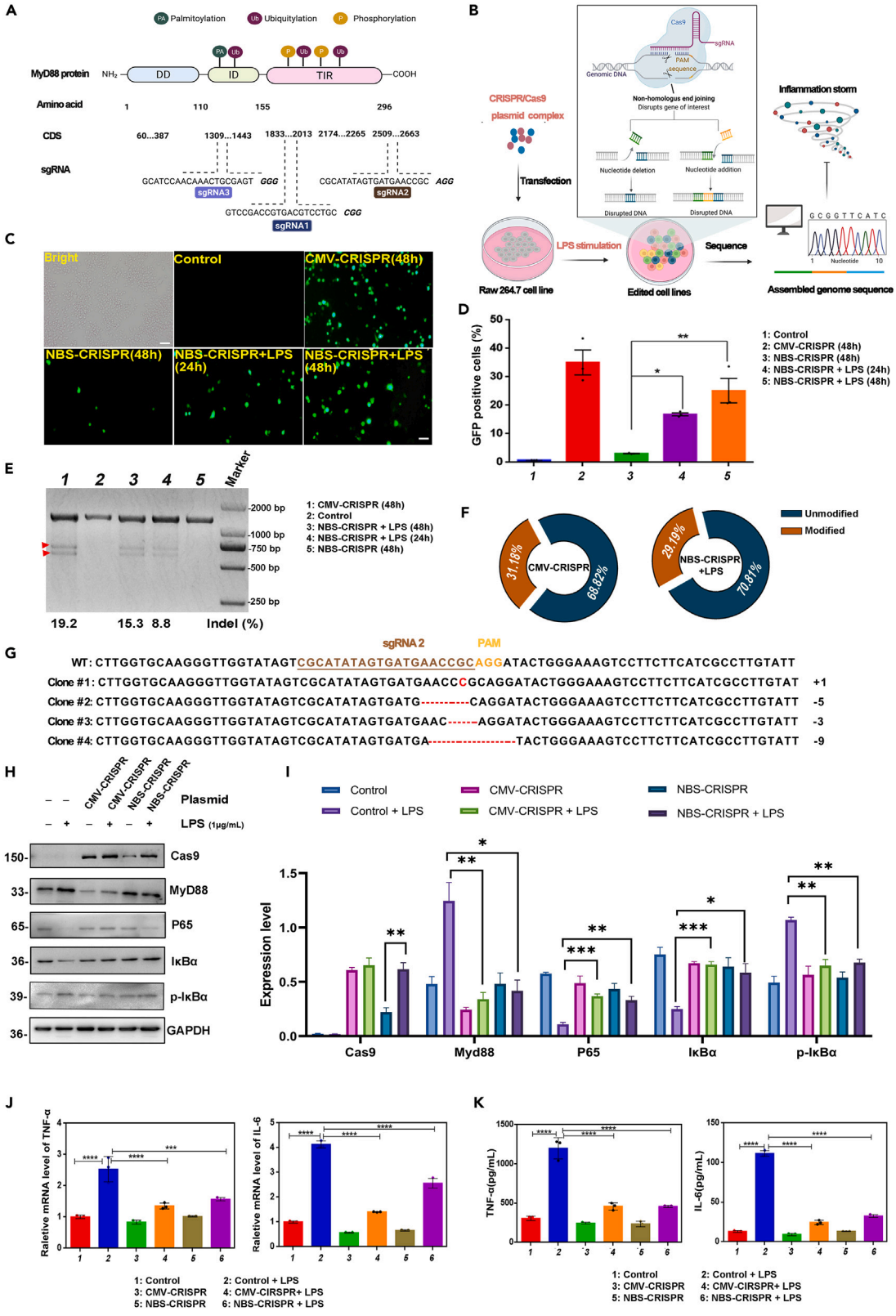
A
Palmitoylation
Ubiquitylation
Phosphorylation
MyD88 protein
DD
ID
TIR
COOH
Amino acid
CDS
sgRNA
GCATCCAACAAACTGCGAGT GGG
sgRNA3
CGCATATAGTGATGAACCGC AGG
sgRNA2
GTCCGACCGTGACGTCCTGC CGG
sgRNA1
B
CRISPR/Cas9
plasmid complex
Transfection
Raw 264.7 cell line
LPS stimulation
Edited cell lines
Sequence
Assembled genome sequence
Inflammation storm
Non-homologus end joining
Disrupts gene of interest
Nucleotide deletion
Nucleotide addition
C
Bright
Control
CMV-CRISPR(48h)
NBS-CRISPR(48h)
NBS-CRISPR+LPS (24h)
NBS-CRISPR+LPS (48h)
D
GFP positive cells (%)
1: Control
2: CMV-CRISPR (48h)
3: NBS-CRISPR (48h)
4: NBS-CRISPR + LPS (24h)
5: NBS-CRISPR + LPS (48h)
E
Marker
2000 bp
1000 bp
750 bp
500 bp
250 bp
19.2
15.3
8.8
Indel (%)
F
Unmodified
Modified
31.18%
68.82%
CMV-CRISPR
29.19%
70.81%
NBS-CRISPR +LPS
G
sgRNA 2
PAM
WT: CTTGGTGCAAGGGTTGGTATAGTCGCATATAGTGATGAACCGCAGGATACTGGGAAAGTCCTTCTTCATCGCCTTGTATT
Clone #1: CTTGGTGCAAGGGTTGGTATAGTCGCATATAGTGATGAACCCGCAGGATACTGGGAAAGTCCTTCTTCATCGCCTTGTAT +1
Clone #2: CTTGGTGCAAGGGTTGGTATAGTCGCATATAGTGATG----------CAGGATACTGGGAAAGTCCTTCTTCATCGCCTTGTATT -5
Clone #3: CTTGGTGCAAGGGTTGGTATAGTCGCATATAGTGATGAAC------AGGATACTGGGAAAGTCCTTCTTCATCGCCTTGTATT -3
Clone #4: CTTGGTGCAAGGGTTGGTATAGTCGCATATAGTGATGA----------TACTGGGAAAGTCCTTCTTCATCGCCTTGTATT -9
H
CMV-CRISPR
CMV-CRISPR
NBS-CRISPR
NBS-CRISPR
Plasmid
LPS (1μg/mL)
150-
Cas9
33-
MyD88
65-
P65
36-
IκBα
39-
p-IκBα
36-
GAPDH
I
Control
Control + LPS
CMV-CRISPR
CMV-CRISPR + LPS
NBS-CRISPR
NBS-CRISPR + LPS
Expression level
Cas9
Myd88
P65
IκBα
p-IκBα
J
Raletive mRNA level of TNF-α
Raletive mRNA level of IL-6
1: Control
2: Control + LPS
3: CMV-CRISPR
4: CMV-CIRSPR+ LPS
5: NBS-CRISPR
6: NBS-CRISPR + LPS
K
TNF-α(pg/mL)
IL-6(pg/mL)
1: Control
2: Control + LPS
3: CMV-CRISPR
4: CMV-CIRSPR+ LPS
5: NBS-CRISPR
6: NBS-CRISPR + LPS

Figure 3. Inflammation-response and interruption of the NBS-CRISPR system in macrophages

(A) Design of sgRNA targeting the *Mus* musculus MyD88 gene.

(B) The workflow of employing the functional CRISPR/Cas9 system in the RAW264.7-cell lines.

(C) Fluorescence microscope image of the RAW264.7 cell line transfected with different functional CRISPR/Cas9 plasmids. NBS, NF-κB binding sequence; CMV-CRISPR, CMV-Cas9-sgRNA2; NBS-CRISPR, NBS-Cas9-sgRNA2. Scale bar: 50 μm.

(D) Quantification of GFP-positive cells in the panel (c). Data are presented as the mean ± SEM (n = 3, *p <0.05, **p < 0.01).

(E) T7E1 assay of DNA cleavage efficiency mediated by the functional CRISPR/Cas9 plasmids.

(F) Deep sequencing analysis of gene editing efficiency mediated by functional CRISPR/Cas9 plasmids.

(G) Illustration of gene modification mediated by functional CRISPR/Cas9 plasmids in edited cells.

(H) Western blotting analysis of Cas9, MyD88, P65, IκBα, p- IκBα protein levels in treated cells. Numbers indicate molecular weight (kDa) of closest molecular weight marker.

(I) Quantification of Cas9, MyD88, P65, IκBα, p- IκBα expression in the panel (H). The repeats of the western blot analysis were repeated from independent experiments. The Data are presented as the mean ± SEM, n = 3. One-way ANOVA with a Tukey's post-hoc test. *p <0.05, **p < 0.01, ***p < 0.001.

(J) mRNA analysis of the pro-inflammatory cytokines IL-6 and TNF-α in treated cells. Data are presented as the mean ± SEM, n = 3. One-way ANOVA with a Tukey's post-hoc test. ***p < 0.001, ****p < 0.0001.

(K) Serum levels of the pro-inflammatory cytokines TNF-α and IL-6 in treated cells. Data are presented as the mean ± SEM, n = 3. One-way ANOVA with a Tukey's post-hoc test. ****p < 0.0001).

in the CMV-CRISPR group (43%), implying that inflammatory activation of this system occurred in macrophages and was time-dependent despite leakage (Figures 3C and 3D). The above results indicate that the NBS-CRISPR system responds well to inflammation in RAW264.7 cells. A subsequent T7 Endonuclease I (T7EI) assay revealed that the MyD88 gene was edited with this functional tool, and its gene editing efficiency (up to 15.3%) was comparable to that of the positive CMV-CRISPR group (19.2%) (Figure 3E). Deep sequencing further identified that the gene editing (29.19%) capabilities of the NBS-CRISPR system are comparable to those of classical CRISPR/Cas9 tools (31.18%) in inflammation condition (Figure 3F); in addition, gene mutations were diverse, including deletions and insertions (Figure 3G).These results confirmed that the NBS-CRISPR system has superior a gene editing performance. Because MyD88 is the canonical adaptor for downstream inflammatory signaling pathways, altering its synthesis could reduce inflammation.[34] Therefore, we next assessed the inflammation status 24 h after transfection with our functional plasmid and 24 h after LPS stimulation. As the western blotting results showed that the expression level of MyD88 was decreased significantly in the NBS-CRISPR plus LPS treated group compared to in the LPS-alone group. With the reduction in MyD88 protein levels, the levels of the downstream protein phosphorylated-inhibitor of nuclear factor κB α (*p*-IκBα) were also decreased, and IκBα and P65 levels were increased (Figures 3H and 3I). Furthermore, the quantitative real-time PCR (qPCR) and enzyme-linked immunosorbent assay (ELISA) results also revealed the moderate secretion of pro-inflammatory cytokines (TNF-α, IL-6) (Figures 3J and 3K) in the edited group. These results illustrated that the reduction of MyD88 alleviated the symptoms of inflammation. Overall, these findings suggest that the inflammation-activated NBS-CRISPR system function well in immune cells and, importantly, abates the inflammatory response because of Myd88 sgRNA targeting.

NBS-CRISPR system validation in primary hepatocytes

We subsequently assessed the performance of our NBS-CRISPR system in primary hepatocytes to evaluate its function in non-immune cells. We isolated primary mouse hepatocytes according to a previously described protocol.[35] All cell samples were collected after the indicted treatments for analysis (Figure 4A). The real-time function of the CRISPR/Cas9 system was verified by monitoring EGFP-positive cells under fluorescence microscope. A luciferase reporter assay was further utilized to detect the luciferase activity, quantitatively reporting the transcriptional activity of NBS induced by inflammation in primary hepatocytes. The results showed that compared with the findings in the NBS-CRISPR plasmid transfection group, the EGFP-positive cell number, fluorescence intensity, and luminescence activity in the NBS-CRISPR plasmid transfection co-LPS induction group were increased significantly and were time-independent (Figures 4B and 4C). Cas9 cleavage activity was further evaluated through a T7EI assay. As anticipated, the maximal indel efficiency was 6.7% in the NBS-CRISPR co-LPS induction group, and that in the positive control group was 10.1% (Figure 4D). Deep sequencing (CMV-CRISPR: 21.47%, NBS-CRISPR + LPS: 13.76%) further confirmed these findings (Figure 4E). Consistent with RAW264.7 cells, the edited cells comprised many clones bearing deletions and insertions (Figure 4F). Western blotting was applied to investigate whether downregulated MyD88 could also attenuate inflammation by reducing the phosphorylation of IκBα. MyD88 level were notably decreased, and the phosphorylation of IκBα was reduced, while the levels of IκBα and P65 increased when LPS was introduced in the NBS-CRISPR group (Figures 4G and 4H). In

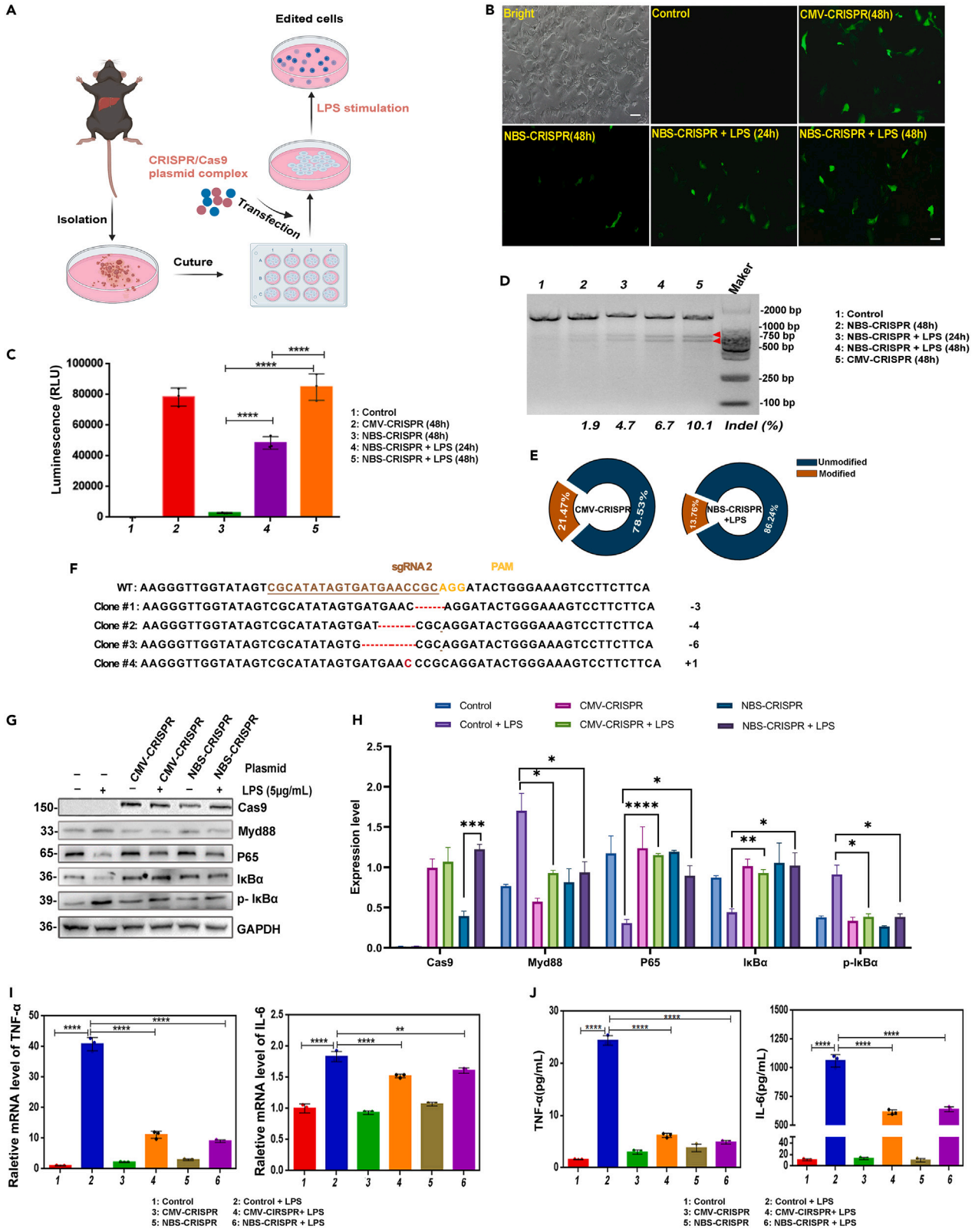
A
Edited cells
LPS stimulation
CRISPR/Cas9
plasmid complex
Transfection
Isolation
Cuture
B
Bright
Control
CMV-CRISPR(48h)
NBS-CRISPR(48h)
NBS-CRISPR + LPS (24h)
NBS-CRISPR + LPS (48h)
C
Luminescence (RLU)
1: Control
2: CMV-CRISPR (48h)
3: NBS-CRISPR (48h)
4: NBS-CRISPR + LPS (24h)
5: NBS-CRISPR + LPS (48h)
D
Maker
-2000 bp
-1000 bp
-750 bp
-500 bp
-250 bp
-100 bp
1.9 4.7 6.7 10.1 Indel (%)
1: Control
2: NBS-CRISPR (48h)
3: NBS-CRISPR + LPS (24h)
4: NBS-CRISPR + LPS (48h)
5: CMV-CRISPR (48h)
E
Unmodified
Modified
CMV-CRISPR
21.47%
78.53%
NBS-CRISPR +LPS
13.76%
86.24%
F
sgRNA 2
PAM
WT: AAGGGTTGGTATAGTCGCATATAGTGATGAACCGCAGGATACTGGGAAAGTCCTTCTTCA
Clone #1: AAGGGTTGGTATAGTCGCATATAGTGATGAAC-------AGGATACTGGGAAAGTCCTTCTTCA -3
Clone #2: AAGGGTTGGTATAGTCGCATATAGTGAT--------CGCAGGATACTGGGAAAGTCCTTCTTCA -4
Clone #3: AAGGGTTGGTATAGTCGCATATAGTG----------CGCAGGATACTGGGAAAGTCCTTCTTCA -6
Clone #4: AAGGGTTGGTATAGTCGCATATAGTGATGAAC CCGCAGGATACTGGGAAAGTCCTTCTTCA +1
G
CMV-CRISPR
CMV-CRISPR
NBS-CRISPR
NBS-CRISPR
Plasmid
LPS (5μg/mL)
Cas9
Myd88
P65
IκBα
p- IκBα
GAPDH
H
Control
Control + LPS
CMV-CRISPR
CMV-CRISPR + LPS
NBS-CRISPR
NBS-CRISPR + LPS
Expression level
Cas9
Myd88
P65
IκBα
p-IκBα
I
Raletive mRNA level of TNF-α
Raletive mRNA level of IL-6
1: Control
2: Control + LPS
3: CMV-CRISPR
4: CMV-CIRSPR+ LPS
5: NBS-CRISPR
6: NBS-CRISPR + LPS
J
TNF-α(pg/mL)
IL-6(pg/mL)
1: Control
2: Control + LPS
3: CMV-CRISPR
4: CMV-CIRSPR+ LPS
5: NBS-CRISPR
6: NBS-CRISPR + LPS

Figure 4. Inflammation-response and interruption of the NBS-CRISPR system in primary hepatocytes

(A) The workflow of evaluating the functional CRISPR/Cas9 system in primary hepatocytes.

(B) Fluorescence microscope image of primary hepatocytes transfected with different functional CRISPR/Cas9 plasmids. NBS, NF-κB binding sequence; CMV-CRISPR, CMV-Cas9-sgRNA2; NBS-CRISPR, NBS-Cas9-sgRNA2.Scale bar: 50 μm.

(C) Analysis of luminescence in panel (B). Data are presented as the mean ± SEM, n = 3. One-way ANOVA with a Tukey's post-hoc test. ****$p < 0.0001$.

(D) T7E1 assay of DNA cleavage efficiency mediated by the functional CRISPR/Cas9 plasmids.

(E) Deep sequencing analysis of gene-editing efficiency mediated by the functional CRISPR/Cas9 plasmids.

(F) Illustration of the gene modification mediated by functional CRISPR/Cas9 plasmids in edited primary hepatocytes.

(G) Western blotting analysis of Cas9, MyD88, P65, IκBα, and p- IκBα protein levels in treated primary hepatocytes. Numbers indicate molecular weight (kDa) of closest molecular weight marker.

(H) Quantification of Cas9, MyD88, P65, IκBα, and p- IκBα expression in the panel (G). The repeats of the western blot analysis were repeated from independent experiments. Data are presented as the mean ± SEM, n = 3. One-way ANOVA with a Tukey's post-hoc test. *$p < 0.05$, **$p < 0.01$, ***$p < 0.001$, ****$p < 0.0001$.

(I) mRNA analysis of the pro-inflammatory cytokines IL-6 and TNF-α in treated primary hepatocytes. Data are presented as the mean ± SEM, n = 3. One-way ANOVA with a Tukey's post-hoc test. **$p < 0.01$, ***$p < 0.001$, ****$p < 0.0001$.

(J) Serum levels of the pro-inflammatory cytokines TNF-α and IL-6 in treated primary hepatocytes. Data are presented as the mean ± SEM, n = 3. One-way ANOVA with a Tukey's post-hoc test. ****$p < 0.0001$.

addition, the quantitative real-time PCR (qPCR) and ELISA results revealed a significant decrease in the secretion of pro-inflammatory factors in the cellular supernatant in the edited group when stimulated with LPS (Figures 4I and 4J). Collectively, these results indicate that our NBS-CRISPR system can be activated by inflammation in primary hepatocytes and alleviate the inflammatory response when the MyD88 sgRNA is Integrated.

The AAV9-NBS-CRISPR system ameliorates liver injury caused by concanavalin A

All of the above results suggested that our NBS-CRISPR system worked well and synchronously alleviated inflammation as a result of MyD88 sgRNA targeting in RAW 264.7 cells and hepatocytes. Thus, we investigated whether this tool could be applied in liver injury. Given the low editing efficiencies of hydrodynamic injection for Cas9 transgene delivery into the mouse liver *in vivo*, we constructed an adeno-associated virus serotype 9 (AAV9) vector with luciferase as the reporter, albeit with the possibility of causing a mild immune response. We employed a dual AAV9 system to deliver the CRISPR transgene because of its limited packaging capacity, one vector carrying Cas9 with the NBS promoter and the other carrying sgRNA2 with the U6 promoter and a luciferase reporter driven by NBS (termed the AAV9-NBS-CRISPR system, completed by ChuangRui Bio Co., China) (Figure 5A). Seven days after intravenous injection of this AAV9 mixture into 4–6-week-old C57/BL6 mice, concanavalin A (Con A) was administered to establish the liver injury model and activate the AAV9-NBS-CRISPR system *in vivo*. The mice intravenously injected with saline and ConA without AAV9 infection were used as negative and positive inflammation controls, respectively. Con A was administrated again 48h later to determine whether the AAV9-NBS-CRISPR system exerts a therapeutic effect on liver injury (Figure 5B). Bioluminescence imaging demonstrated that although AAV9 intravenous injection caused a mild inflammatory response, our system showed a more robust luminescence intensity when Con A was administered (Figures 5C and 5D). Indeed, we observed that enhanced luminescence was mainly localized in the liver (Figures 5E and 5F). From the T7EI results, we concluded this NBS promoter-mediated inflammation-control of Cas9 enables genome-interrogating activities of our AAV9-NBS-CRISPR system (Figure 5G). Next, we observed that alanine aminotransferase (ALT) and aspartate aminotransferase (AST) levels were dramatically decreased in the AAV9-NBS-CRISPR-treated model, suggesting that it alleviated ConA-induced liver injury (Figure 5H). The extent of liver damage was further assessed by histology. The HE staining results confirmed that the reduction in MyD88 prevented ConA-induced liver damage (Figures 5I and 5J). Overall, we validated that our NBS-CRISPR workflow can be triggered by inflammation and reversely ameliorate inflammation *in vivo*.

Optimization of the NBS-CRISPR system

Given the leaky Cas9 expression of NBS-CRISPR system, we further aimed to locate Cas9 in the cytoplasm, thereby weakening its cleavage activity, in the absence of inflammation. The P50/P65 heterodimer is an essential subunit for NF-κB complexes that normally retained in the cytosol in an inactive form with IκBα, an inhibitor which masks the p65-nuclear localization sequence (NLS). Upon activation, p50/p65 is translocated into the nucleus under the guidance of P65-NLS after IκBα is phosphorylated and degraded in the proteasome.[36] On this basis, the corresponding human p65 code sequence was assembled into the NBS-CRISPR system. Considering that other NLSs may transport Cas9 to the nucleus, we constructed two

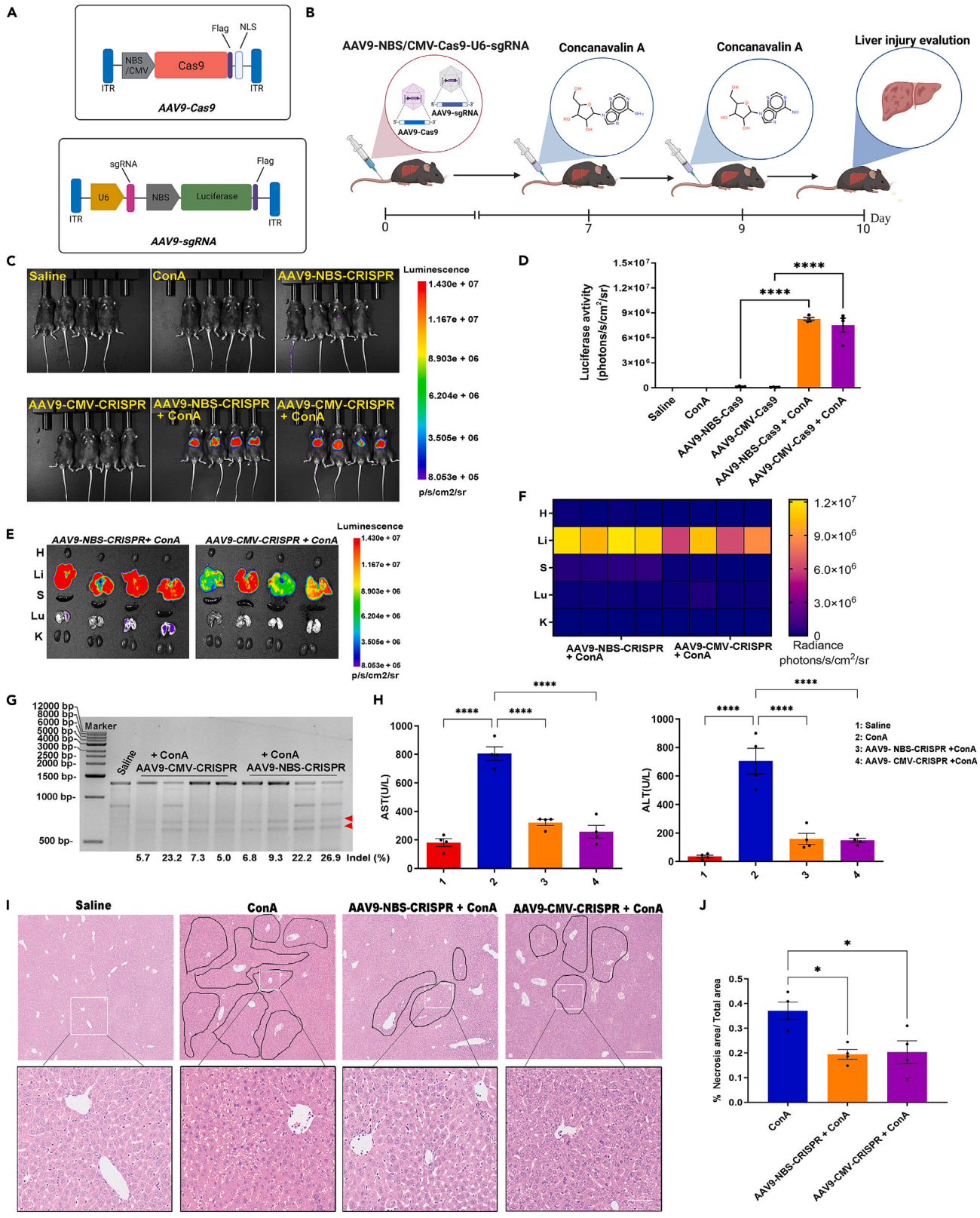
A
Flag
NLS
NBS /CMV
Cas9
ITR
ITR
AAV9-Cas9
sgRNA
Flag
U6
NBS
Luciferase
ITR
ITR
AAV9-sgRNA
B
AAV9-NBS/CMV-Cas9-U6-sgRNA
Concanavalin A
Concanavalin A
Liver injury evalution
AAV9-sgRNA
AAV9-Cas9
0
7
9
10
Day
C
Saline
ConA
AAV9-NBS-CRISPR
AAV9-CMV-CRISPR
AAV9-NBS-CRISPR + ConA
AAV9-CMV-CRISPR + ConA
Luminescence
1.430e + 07
1.167e + 07
8.903e + 06
6.204e + 06
3.505e + 06
8.053e + 05
p/s/cm2/sr
D
Luciferase avtivity (photons/s/cm2/sr)
1.5×10^7
1.2×10^7
9×10^6
6×10^6
3×10^6
0
****
****
Saline
ConA
AAV9-NBS-Cas9
AAV9-CMV-Cas9
AAV9-NBS-Cas9 + ConA
AAV9-CMV-Cas9 + ConA
E
AAV9-NBS-CRISPR+ ConA
AAV9-CMV-CRISPR + ConA
H
Li
S
Lu
K
Luminescence
1.430e + 07
1.167e + 07
8.903e + 06
6.204e + 06
3.505e + 06
8.053e + 05
p/s/cm2/sr
F
H
Li
S
Lu
K
AAV9-NBS-CRISPR + ConA
AAV9-CMV-CRISPR + ConA
1.2×10^7
9.0×10^6
6.0×10^6
3.0×10^6
0
Radiance photons/s/cm2/sr
G
12000 bp
8000 bp
6000 bp
5000 bp
4000 bp
3000 bp
2500 bp
2000 bp
1500 bp
1000 bp
500 bp
Marker
Saline
+ ConA AAV9-CMV-CRISPR
+ ConA AAV9-NBS-CRISPR
5.7 23.2 7.3 5.0 6.8 9.3 22.2 26.9 Indel (%)
H
AST(U/L)
ALT(U/L)
****
****
****
1: Saline
2: ConA
3: AAV9- NBS-CRISPR +ConA
4: AAV9- CMV-CRISPR +ConA
I
Saline
ConA
AAV9-NBS-CRISPR + ConA
AAV9-CMV-CRISPR + ConA
J
% Necrosis area/ Total area
0.5
0.4
0.3
0.2
0.1
0.0
*
*
ConA
AAV9-NBS-CRISPR + ConA
AAV9-CMV-CRISPR + ConA

Figure 5. The AAV9-NBS-CRISPR system could ameliorate liver injury caused by concanavalin A (Con A)

(A) Strategy for the construction of the AAV9-NBS-CRISPR system.

(B) Experimental scheme of AAV9-NBS-CRISPR therapy for acute liver injury.

(C) Examination of luciferase expression after AAV9 mixture tail intravenous injection and Con A administration (n = 4).

(D) Quantification of the luminescence intensity in panel (C). Data are presented as the mean ± SEM, n = 4. One-way ANOVA with a Tukey's post-hoc test. ****$p < 0.0001$.

(E) Biodistribution of luciferase expression in panel (C). H, Heart; Li, Liver; S, Spleen; Lu, Lung; K, Kidney.

(F) Quantification of the luminescence intensity in panel (E).

(G) T7E1 assay of DNA cleavage efficiency mediated by the AAV9-CMV/NBS-CRISPR system.

(H) Measurement of serum ALT and AST levels in the control and treated groups. Data are presented as the mean ± SEM, n = 4. One-way ANOVA with a Tukey's post-hoc test. ****$p < 0.0001$.

(I) Histological analysis of liver tissue through HE staining. The black dash line denoted the area of liver damage and tissue necrosis. Scar bar, top panel, 200 μm; scar bar, lower panel, 25μm.

(J) Quantification of the necrosis area (% of the total area) in panel (I). Data are presented as the mean ± SEM, n = 4. One-way ANOVA with a Tukey's post-hoc test. *$p < 0.05$).

vectors encoding the Cas9-P65 hybrid protein with 3× GGGGS[37] linkage and mCherry as the reporter, referred to NBS-P65 I-CRISPR (with SV40 NLS tagged 5′-Cas9) and NBS-P65 II-CRISPR (Figure 6A). We expected that hybrid P65 in the cytoplasm with IκBα protein masking would simultaneously trap Cas9 protein in the cytosol under normal conditions. After incorporating human p65, we designed sgRNAs targeting the human MyD88 gene and picked the sgRNA4 for subsequent assays evaluating DNA cleavage efficiency (Figure S6). Twenty-four hours after transfection into HEK293T cells, the medium was changed to complete medium supplemented with 50 ng/mL TNF-α. Thereafter, the cells were cultured at 37°C in 5% CO2 for an additional 24 h. Fluorescence confocal microscopy imaging was then performed (Figure 6B). As expected, in the NBS-P65 I/II-CRISPR with or without TNFα challenge groups, the location of mCherry indicated that Cas9 was successfully retained in the cytoplasm under normal circumstances but was shuttled into the nucleus during inflammation (Figure 6C). However, in the NBS-CRISPR group, Cas9 immunofluorescence staining revealed that at it was located nucleus and cytoplasm (Figure 6C). In addition, there were no significant differences between the NBS-P65 I-CRISPR group and the NBS-P65 II-CRISPR group. The Western blot results showed a larger Cas9 molecular weight indicated that when P65 was fused, and this fusion protein was expressed at higher levels under TNF-α stimulation (Figure 6D). Ideally, the T7E1 assay illustrated that leaky genome cleavage of NBS-CRISPR was controlled by P65 infusion (the editing efficiency decreased from 2.1% to 0.4%) (Figure 6E). Collectively, these data indicate that the tested strategy is effective for reducing leaky Cas9 cleavage activity in NBS-CRISPR system and shows potential for application in other CRISPR orthologs.

DISCUSSION

Inflammation, the main culprit in numerous disorders, has long been a critical therapeutic target. Thus, here we established an inflammation-induced CRISPR/Cas9 system possessing high gene editing efficiency comparable to that of a ubiquitous promoter (CMV)-driven system. In our system, we placed NBS upstream of Cas9; NF-κB translocates to the nucleus from the cytoplasm in response to infection or injury and further binds to the NBS, activating Cas9 expression and initiating gene editing guided by the target sgRNA. We first validated our system *in vitro* in RAW 264.7 cells and primary hepatocytes (Figures 3, 4). The results showed that the system is effectively activated by inflammation. *In vivo* experiments were conducted to further validate our findings (Figure 5). We next sought to determine whether this system can reverse inflammation. Therefore, we picked the most efficient sgRNA for targeting the MyD88 gene and inserted it into our NBS-CRISPR vector. As expected, the disruption of MyD88 indeed ameliorated the inflammatory response, similar to a circuit that is triggered by inflammation and in turn eliminates it. The capability of our NBS-CRISPR system to manipulate the MyD88 gene in a ConA-induced liver injury is also highly desirable (Figure 5).

We found leaky Cas9 expression during the course of the study. The P50/P65 heterodimer is a typical factor, and P65 functions as the limiting component of NF-κB signaling pathway-associated shuttling between the cytoplasm and nucleus[29]; thus we hypothesized that combining p65 with Cas9 would limit Cas9 localization. In contrast to the PB-SAM system, in which the C-terminus of P65 subunit was introduced to recruit a distinct subset of transcription factors, such as AP-1, CREB and SP1,[38–40] we combined the complete P65 protein, including the NLS motif, to form the IκBα binding pocket. Inducers result in the phosphorylation and degradation of IκBα, releasing the NLS motif, thus allowing P65-Cas9 fusion protein nuclear

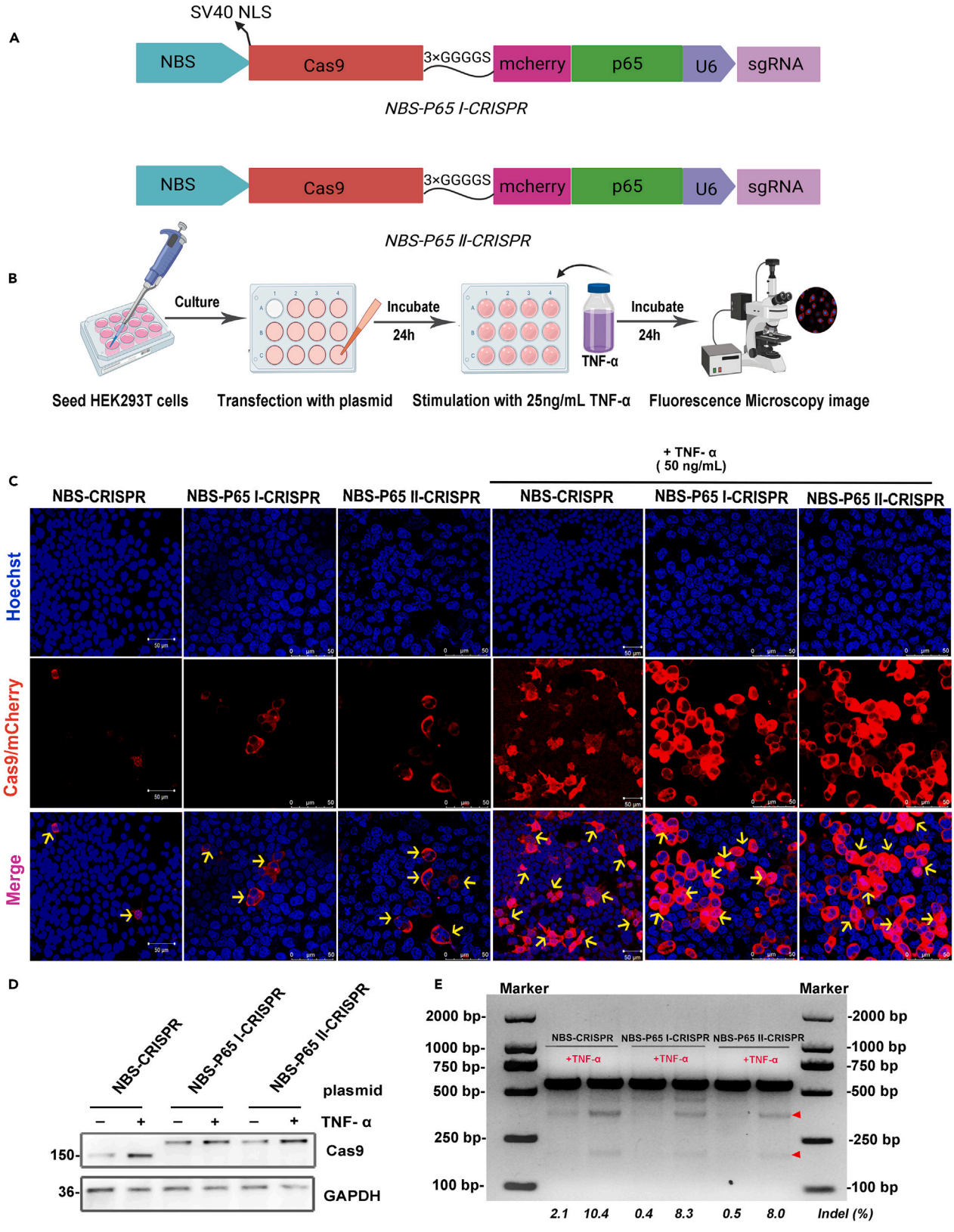
A
SV40 NLS
NBS
Cas9
3×GGGGS
mcherry
p65
U6
sgRNA
NBS-P65 I-CRISPR
NBS
Cas9
3×GGGGS
mcherry
p65
U6
sgRNA
NBS-P65 II-CRISPR
B
Culture
Incubate
24h
Incubate
24h
TNF-α
Seed HEK293T cells
Transfection with plasmid
Stimulation with 25ng/mL TNF-α
Fluorescence Microscopy image
C
+ TNF- α
(50 ng/mL)
NBS-CRISPR
NBS-P65 I-CRISPR
NBS-P65 II-CRISPR
NBS-CRISPR
NBS-P65 I-CRISPR
NBS-P65 II-CRISPR
Hoechst
Cas9/mCherry
Merge
D
NBS-CRISPR
NBS-P65 I-CRISPR
NBS-P65 II-CRISPR
plasmid
– + – + – +
TNF- α
150-
Cas9
36-
GAPDH
E
Marker
Marker
2000 bp-
1000 bp-
750 bp-
500 bp-
250 bp-
100 bp-
NBS-CRISPR
NBS-P65 I-CRISPR
NBS-P65 II-CRISPR
+TNF-α
+TNF-α
+TNF-α
-2000 bp
-1000 bp
-750 bp
-500 bp
-250 bp
-100 bp
2.1 10.4 0.4 8.3 0.5 8.0
Indel (%)

Figure 6. Optimization of the NBS-CRISPR system

(A) Construction of the optimized NBS-P65 I-CRISPR and NBS-P65 II-CRISPR systems.

(B) Experimental scheme of conducting the NBS-P65 I-CRISPR and NBS-P65 II-CRISPR systems in HEK 293T cells.

(C) Confocal fluorescence microscopic images of the localization of mCherry and Cas9. Scale bar: 50 μm.

(D) Western blotting analysis of Cas9 levels in HEK293T cells. Numbers indicate molecular weight (kDa) of closest molecular weight marker.

(E) T7E1 assay of DNA cleavage efficiency mediated by the NBS-CRISPR, NBS-P65 I-CRISPR and NBS-P65 II-CRISPR systems.

translocation. However, P65-Cas9 fusion protein is retained in the cytoplasm on association with IκBα in most cells and under non-inflammatory conditions. Hence, the results also verified that the leaky DNA cleavage activity could be minimized (Figure 6E).

The generation of NBS-CRISPR and NBS-P65I/II-CRISPR systems provides a platform for therapeutic gene editing, especially for inflammation-related diseases. These systems can limit genome interrogation to lesion-specific sites through endogenous pathological processes that trigger Cas9, thus reducing damage to surrounding tissues and further lowering off-target risk. Recently, we also reviewed a report where described a Cas13a system controlled by an NF-κB-specific promoter for interfering with cancer progression, and this approach achieved impressive results.[41]

To date, many stimuli-response non-viral CRISPR platforms have been developed, and nanoparticles are commonly incorporated. These stimuli include internal environmental cues, such as PH and reactive oxygen species (ROS), and external inducers, such as light, heat, and magnetism.[42] AAV vector have be applied in clinical (eg. the drugs, Glybera, LUXTURNA and ZOLGENSMA)[43]; however, the controllable viral delivery system should also be enhanced. AAV is the leading platform for *in vivo* gene therapy, and there is substantial promise for deploying AAV-based CRISPR toolbox. However, there are limitations associated with using AAV vectors to deliver CRISPR systems, such as the low gene loading capacity and uncontrollability.[44] Long-term Cas9 expression from AAVs *in vivo* will lead to undesired outcomes (e.g., off-targets). Herein, we expect that the combination of our NBS-CRISPR system with AAV platform will achieve spatial control of CRISPR-based AAV therapeutics for inflammatory disease and associated disorders.

Limitations of the study

Although our NBS-CRISPR system can respond sensitively to acute inflammation and possess superior gene interrogation capabilities, there are still some limitations, (1) Validation of its feasibility in other CRISPR orthologs (e.g., CRISPR-dCas9 system, ABE/CBE/PE base editor system[45] has not been conducted. (2) Verification of its therapeutic effect on chronic inflammatory disorders (such as atherosclerosis) remains to be carried out. At all events, we expect that the present research will inspire a better understanding of CRISPR/Cas9 to be exploited for specific inflammatory diseases.

STAR★METHODS

Detailed methods are provided in the online version of this paper and include the following:

- KEY RESOURCES TABLE
- RESOURCE AVAILABILITY
  - Lead contact
  - Materials availability
  - Data and code availability
- EXPERIMENTAL MODEL AND SUBJECT DETAILS
  - Cell lines
  - Animals
- METHOD DETAILS
  - Construction of functional plasmids
  - Cell culture
  - Cell transfection
  - Inflammation stimulation
  - Gene editing assay
  - T7EI assay
  - Real-time PCR (qPCR)
  - Western blotting

- Enzyme-linked immunosorbent assay (ELISA)
- Luciferase assay
- Animal experiments
- Inclusion and exclusion criteria

- QUANTIFICATION AND STATISTICAL ANALYSIS

SUPPLEMENTAL INFORMATION

Supplemental information can be found online at https://doi.org/10.1016/j.isci.2023.106872.

ACKNOWLEDGMENTS

This work was supported by Zhejiang Provincial Key Research Project (2021C03041) and National Natural Science Foundation of China (81930108).

AUTHOR CONTRIBUTIONS

G.L., Y.P., and Y-C.C. conceived the project, designed the methodology and supervised manuscript. T.T.Y., L.H.T., and J.X.X. performed the experiments. G.L. and T.T analyzed the data, wrote and revised the manuscript, J.J.S. and G.J.W. analyzed the data.

DECLARATION OF INTERESTS

The authors declare no competing interests.

Received: October 16, 2022
Revised: February 3, 2023
Accepted: May 9, 2023
Published: May 13, 2023

REFERENCES

1. Quail, D.F., Amulic, B., Aziz, M., Barnes, B.J., Eruslanov, E., Fridlender, Z.G., Goodridge, H.S., Granot, Z., Hidalgo, A., Huttenlocher, A., et al. (2022). Neutrophil phenotypes and functions in cancer: A consensus statement. J. Exp. Med. *219*, e20220011. https://doi.org/10.1084/jem.20220011.

2. Castellanos, J.G., and Longman, R.S. (2019). The balance of power: innate lymphoid cells in tissue inflammation and repair. J. Clin. Invest. *129*, 2640–2650. https://doi.org/10.1172/JCI124617.

3. Nedeva, C., Menassa, J., Duan, M., Liu, C., Doerflinger, M., Kueh, A.J., Herold, M.J., Fonseka, P., Phan, T.K., Faou, P., et al. (2020). TREML4 receptor regulates inflammation and innate immune cell death during polymicrobial sepsis. Nat. Immunol. *21*, 1585–1596. https://doi.org/10.1038/s41590-020-0789-z.

4. Rohm, T.V., Meier, D.T., Olefsky, J.M., and Donath, M.Y. (2022). Inflammation in obesity, diabetes, and related disorders. Immunity *55*, 31–55. https://doi.org/10.1016/j.immuni.2021.12.013.

5. Hammond, T.R., Marsh, S.E., and Stevens, B. (2019). Immune signaling in neurodegeneration. Immunity *50*, 955–974. https://doi.org/10.1016/j.immuni.2019.03.016.

6. Jacquelot, N., Seillet, C., Vivier, E., and Belz, G.T. (2022). Innate lymphoid cells and cancer. Nat. Immunol. *23*, 371–379. https://doi.org/10.1038/s41590-022-01127-z.

7. Skaug, B., Jiang, X., and Chen, Z.J. (2009). The role of ubiquitin in NF-kappaB regulatory pathways. Annu. Rev. Biochem. *78*, 769–796. https://doi.org/10.1146/annurev.biochem.78.070907.102750.

8. Zhang, Q., Lenardo, M.J., and Baltimore, D. (2017). 30 Years of NF-kappaB: a blossoming of relevance to human pathobiology. Cell *168*, 37–57. https://doi.org/10.1016/j.cell.2016.12.012.

9. Jiang, F., and Doudna, J.A. (2017). CRISPR-Cas9 structures and mechanisms. Annu. Rev. Biophys. *46*, 505–529. https://doi.org/10.1146/annurev-biophys-062215-010822.

10. Platt, R.J., Chen, S., Zhou, Y., Yim, M.J., Swiech, L., Kempton, H.R., Dahlman, J.E., Parnas, O., Eisenhaure, T.M., Jovanovic, M., et al. (2014). CRISPR-Cas9 knockin mice for genome editing and cancer modeling. Cell *159*, 440–455. https://doi.org/10.1016/j.cell.2014.09.014.

11. Zetsche, B., Volz, S.E., and Zhang, F. (2015). A split-Cas9 architecture for inducible genome editing and transcription modulation. Nat. Biotechnol. *33*, 139–142. https://doi.org/10.1038/nbt.3149.

12. Truong, D.J.J., Kühner, K., Kühn, R., Werfel, S., Engelhardt, S., Wurst, W., and Ortiz, O. (2015). Development of an intein-mediated split-Cas9 system for gene therapy. Nucleic Acids Res. *43*, 6450–6458. https://doi.org/10.1093/nar/gkv601.

13. Aubrey, B.J., Kelly, G.L., Kueh, A.J., Brennan, M.S., O'Connor, L., Milla, L., Wilcox, S., Tai, L., Strasser, A., and Herold, M.J. (2015). An inducible lentiviral guide RNA platform enables the identification of tumor-essential genes and tumor-promoting mutations in vivo. Cell Rep. *10*, 1422–1432. https://doi.org/10.1016/j.celrep.2015.02.002.

14. Liu, K.I., Ramli, M.N.B., Woo, C.W.A., Wang, Y., Zhao, T., Zhang, X., Yim, G.R.D., Chong, B.Y., Gowher, A., Chua, M.Z.H., et al. (2016). A chemical-inducible CRISPR-Cas9 system for rapid control of genome editing. Nat. Chem. Biol. *12*, 980–987. https://doi.org/10.1038/nchembio.2179.

15. Yu, Y., Wu, X., Guan, N., Shao, J., Li, H., Chen, Y., Ping, Y., Li, D., and Ye, H. (2020). Engineering a far-red light-activated split-Cas9 system for remote-controlled genome editing of internal organs and tumors. Sci. Adv. *6*, eabb1777. https://doi.org/10.1126/sciadv.abb1777.

16. Balboa, D., Weltner, J., Eurola, S., Trokovic, R., Wartiovaara, K., and Otonkoski, T. (2015). Conditionally stabilized dCas9 activator for controlling gene expression in human cell reprogramming and differentiation. Stem Cell Rep. *5*, 448–459. https://doi.org/10.1016/j.stemcr.2015.08.001.

17. Chavez, A., Scheiman, J., Vora, S., Pruitt, B.W., Tuttle, M., P R Iyer, E., Lin, S., Kiani, S.,

Guzman, C.D., Wiegand, D.J., et al. (2015). Highly efficient Cas9-mediated transcriptional programming. Nat. Methods *12*, 326–328. https://doi.org/10.1038/nmeth.3312.

18. Maji, B., Moore, C.L., Zetsche, B., Volz, S.E., Zhang, F., Shoulders, M.D., and Choudhary, A. (2017). Multidimensional chemical control of CRISPR-Cas9. Nat. Chem. Biol. *13*, 9–11. https://doi.org/10.1038/nchembio.2224.

19. Lu, J., Zhao, C., Zhao, Y., Zhang, J., Zhang, Y., Chen, L., Han, Q., Ying, Y., Peng, S., Ai, R., and Wang, Y. (2018). Multimode drug inducible CRISPR/Cas9 devices for transcriptional activation and genome editing. Nucleic Acids Res. *46*, e25. https://doi.org/10.1093/nar/gkx1222.

20. Gemberling, M.P., Siklenka, K., Rodriguez, E., Tonn-Eisinger, K.R., Barrera, A., Liu, F., Kantor, A., Li, L., Cigliola, V., Hazlett, M.F., et al. (2021). Transgenic mice for in vivo epigenome editing with CRISPR-based systems. Nat. Methods *18*, 965–974. https://doi.org/10.1038/s41592-021-01207-2.

21. Kampmann, M. (2018). CRISPRi and CRISPRa screens in mammalian cells for precision biology and medicine. ACS Chem. Biol. *13*, 406–416. https://doi.org/10.1021/acschembio.7b00657.

22. Chylinski, K., Hubmann, M., Hanna, R.E., Yanchus, C., Michlits, G., Uijttewaal, E.C.H., Doench, J., Schramek, D., and Elling, U. (2019). CRISPR-Switch regulates sgRNA activity by Cre recombination for sequential editing of two loci. Nat. Commun. *10*, 5454. https://doi.org/10.1038/s41467-019-13403-y.

23. Kundert, K., Lucas, J.E., Watters, K.E., Fellmann, C., Ng, A.H., Heineike, B.M., Fitzsimmons, C.M., Oakes, B.L., Qu, J., Prasad, N., et al. (2019). Controlling CRISPR-Cas9 with ligand-activated and ligand-deactivated sgRNAs. Nat. Commun. *10*, 2127. https://doi.org/10.1038/s41467-019-09985-2.

24. Jain, S., Xun, G., Abesteh, S., Ho, S., Lingamaneni, M., Martin, T.A., Tasan, I., Yang, C., and Zhao, H. (2021). Precise regulation of cas9-mediated genome engineering by anti-CRISPR-based inducible CRISPR controllers. ACS Synth. Biol. *10*, 1320–1327. https://doi.org/10.1021/acssynbio.0c00548.

25. Lin, J., Wang, W.J., Wang, Y., Liu, Y., and Xu, L. (2021). Building endogenous gene connections through RNA self-assembly controlled CRISPR/Cas9 function. J. Am. Chem. Soc. *143*, 19834–19843. https://doi.org/10.1021/jacs.1c09041.

26. Liu, X., Xiong, W., Qi, Q., Zhang, Y., Ji, H., Cui, S., An, J., Sun, X., Yin, H., Tian, T., and Zhou, X. (2022). Rational guide RNA engineering for small-molecule control of CRISPR/Cas9 and gene editing. Nucleic Acids Res. *50*, 4769–4783. https://doi.org/10.1093/nar/gkac255.

27. Alcoceba, M., García-Álvarez, M., Medina, A., Maldonado, R., González-Calle, V., Chillón, M.C., Sarasquete, M.E., González, M., García-Sanz, R., and Jiménez, C. (2022). MYD88 mutations: transforming the landscape of IgM monoclonal gammopathies. Int. J. Mol. Sci. *23*, 5570. https://doi.org/10.3390/ijms23105570.

28. Yan, S., Fu, Q., Zhou, Y., Zhang, N., Zhou, Q., Wang, X., Yuan, Z., Wang, X., Du, J., Zhang, J., and Zhan, L. (2013). Establishment of stable reporter expression for in vivo imaging of nuclear factor-kappaB activation in mouse liver. Theranostics *3*, 841–850. https://doi.org/10.7150/thno.6997.

29. Smith, E.L., Somma, D., Kerrigan, D., McIntyre, Z., Cole, J.J., Liang, K.L., Kiely, P.A., Keeshan, K., and Carmody, R.J. (2019). The regulation of sequence specific NF-kappaB DNA binding and transcription by IKKbeta phosphorylation of NF-kappaB p50 at serine 80. Nucleic Acids Res. *47*, 11151–11163. https://doi.org/10.1093/nar/gkz873.

30. Kim, S., Kim, D., Cho, S.W., Kim, J., and Kim, J.S. (2014). Highly efficient RNA-guided genome editing in human cells via delivery of purified Cas9 ribonucleoproteins. Genome Res. *24*, 1012–1019. https://doi.org/10.1101/gr.171322.113.

31. Wen, Y., Lambrecht, J., Ju, C., and Tacke, F. (2021). Hepatic macrophages in liver homeostasis and diseases-diversity, plasticity and therapeutic opportunities. Cell. Mol. Immunol. *18*, 45–56. https://doi.org/10.1038/s41423-020-00558-8.

32. Campana, L., Esser, H., Huch, M., and Forbes, S. (2021). Liver regeneration and inflammation: from fundamental science to clinical applications. Nat. Rev. Mol. Cell Biol. *22*, 608–624. https://doi.org/10.1038/s41580-021-00373-7.

33. Ve, T., Vajjhala, P.R., Hedger, A., Croll, T., DiMaio, F., Horsefield, S., Yu, X., Lavrencic, P., Hassan, Z., Morgan, G.P., et al. (2017). Structural basis of TIR-domain-assembly formation in MAL- and MyD88-dependent TLR4 signaling. Nat. Struct. Mol. Biol. *24*, 743–751. https://doi.org/10.1038/nsmb.3444.

34. Kim, Y.C., Lee, S.E., Kim, S.K., Jang, H.D., Hwang, I., Jin, S., Hong, E.B., Jang, K.S., and Kim, H.S. (2019). Toll-like receptor mediated inflammation requires FASN-dependent MYD88 palmitoylation. Nat. Chem. Biol. *15*, 907–916. https://doi.org/10.1038/s41589-019-0344-0.

35. Charni-Natan, M., and Goldstein, I. (2020). Protocol for primary mouse hepatocyte isolation. STAR Protoc. *1*, 100086. https://doi.org/10.1016/j.xpro.2020.100086.

36. Florio, T.J., Lokareddy, R.K., Yeggoni, D.P., Sankhala, R.S., Ott, C.A., Gillilan, R.E., and Cingolani, G. (2022). Differential recognition of canonical NF-kappaB dimers by Importin alpha3. Nat. Commun. *13*, 1207. https://doi.org/10.1038/s41467-022-28846-z.

37. Zhang, X., Zhu, B., Chen, L., Xie, L., Yu, W., Wang, Y., Li, L., Yin, S., Yang, L., Hu, H., et al. (2020). Dual base editor catalyzes both cytosine and adenine base conversions in human cells. Nat. Biotechnol. *38*, 856–860. https://doi.org/10.1038/s41587-020-0527-y.

38. Konermann, S., Brigham, M.D., Trevino, A.E., Joung, J., Abudayyeh, O.O., Barcena, C., Hsu, P.D., Habib, N., Gootenberg, J.S., Nishimasu, H., et al. (2015). Genome-scale transcriptional activation by an engineered CRISPR-Cas9 complex. Nature *517*, 583–588. https://doi.org/10.1038/nature14136.

39. Li, S., Zhang, A., Xue, H., Li, D., and Liu, Y. (2017). One-step piggyBac transposon-based CRISPR/Cas9 activation of multiple genes. Mol. Ther. Nucleic Acids *8*, 64–76. https://doi.org/10.1016/j.omtn.2017.06.007.

40. Qiang, L., Yang, S., Cui, Y.H., and He, Y.Y. (2021). Keratinocyte autophagy enables the activation of keratinocytes and fibroblastsand facilitates wound healing. Autophagy *17*, 2128–2143. https://doi.org/10.1080/15548627.2020.1816342.

41. Gao, J., Luo, T., and Wang, J. (2021). Gene interfered-ferroptosis therapy for cancers. Nat. Commun. *12*, 5311. https://doi.org/10.1038/s41467-021-25632-1.

42. Fang, T., Cao, X., Ibnat, M., and Chen, G. (2022). Stimuli-responsive nanoformulations for CRISPR-Cas9 genome editing. J. Nanobiotechnol. *20*, 354. https://doi.org/10.1186/s12951-022-01570-y.

43. Nidetz, N.F., McGee, M.C., Tse, L.V., Li, C., Cong, L., Li, Y., and Huang, W. (2020). Adeno-associated viral vector-mediated immune responses: understanding barriers to gene delivery. Pharmacol. Ther. *207*, 107453. https://doi.org/10.1016/j.pharmthera.2019.107453.

44. Wang, D., Zhang, F., and Gao, G. (2020). CRISPR-based therapeutic genome editing: strategies and in vivo delivery by AAV vectors. Cell *181*, 136–150. https://doi.org/10.1016/j.cell.2020.03.023.

45. Koblan, L.W., Doman, J.L., Wilson, C., Levy, J.M., Tay, T., Newby, G.A., Maianti, J.P., Raguram, A., and Liu, D.R. (2018). Improving cytidine and adenine base editors by expression optimization and ancestral reconstruction. Nat. Biotechnol. *36*, 843–846. https://doi.org/10.1038/nbt.4172.

STAR★METHODS

KEY RESOURCES TABLE

REAGENT or RESOURCE	SOURCE	IDENTIFIER
Antibodies		
CRISPR-Cas9 Mouse Monoclonal Antibody	Beyotime	Cat# AF0123
FLAG Tag Rabbit Polyclonal Antibody	Affinity	Cat# T0053
MyD88 (D80F5) Rabbit mAb	Cell Signaling Technology	Cat# 4283
NF-κB p65 Rabbit Polyclonal antibody	Proteintech	Cat# 10745-1-AP
IκB Alpha Mouse Monoclonal antibody	Proteintech	Cat# 66418-1-Ig
Phospho-NF-κB p65(Ser536) Ab	Affinity	Cat# AF2006
GAPDH Mouse Monoclonal antibody	Proteintech	Cat# 60004-1-IG
goat anti-mouse IgG (H + L), HRP conjugate	Proteintech	Cat# SA00001-1
goat anti-Rabbit IgG (H + L), HRP conjugate	Proteintech	Cat# SA00001-2
Bacterial and virus strains		
CMV-Cas9-P2A-GFP-P2A-luciferase-pA	Addgene	Cat# 48138
pCmv-mCherry-p65	Beyotime	Cat# D2821
Trelief® 5α Chemically Competent cell	TSINGKE	Cat# TSC-C01
AAV9 vectors	ChuangRui Bio Co. China	N/A
Chemicals, peptides, and recombinant proteins		
Lipo8000™ Transfection Reagent	Beyotime	Cat# C0533
Lipofectamine™ 3000 Reagent	Invitrogen	Cat# L3000015
NATE™ Nucleic acid transfection enhancer	InvivoGen	Cat code: lyec-nate
Lipopolysaccharides(LPS)	Solarbio® LIFE SCIENCES	Cat# L8880
Recombinant Human TNF-α	PEPROTECH	Cat# 300-01A
SN50	MedChemExpress	Cat# HYP0151
D-luciferase postassium salt	Beyotime	Cat# ST196
Critical commercial assays		
T7 Endonuclease I Buffer	NEW ENGLAND BioLabs	Cat# M0302S
RIPA Lysis Buffer	Servicebio	Cat# G2002
Pierce™ Rapid Gold BCA	Thermo Scientific™	Cat# A53226
KOD FX	TOYOBO	Cat# KFX-101
FastPure Cell/Tissue DNA Isolation Mini Kit	Vazyme	Cat# DC102-01
FastPure Gel DNA Extraction Mini Kit	Vazyme	Cat# DC301
Hieff® qPCR SYBR® Green Master Mix (Low Rox)	YEASEN	Cat# 11202ES03/08/60
HiScript® III RT Super-Mix for Qpcr (+gDNA wiper)	Vazyme	Cat# R323-01
Oligonucleotides		
Oligonucleotides used in this study, see TableS1	This paper	N/A
Software and algorithms		
ImageJ software	NIH	https://imagej.nih.gov/ij/
Graphpadprism 9.0.0 software	Graph Pad Software	https://www.graphpad.com/scientific software/prism/
SnapGene® 4.3.6	SnapGene by Dotmatics	https://www.snapgene.com/

RESOURCE AVAILABILITY

Lead contact

Further information and requests for resources and reagents should be directed to and will be fulfilled by the lead contact, wzmcliangguang@163.com (Guang Liang)

Materials availability

This study did not generate new unique reagents.

Data and code availability

Data reported in this paper will be shared by the lead contact upon request. This paper does not report original code. Any reasonable information request for the data reported in this paper is available from the lead contact.

EXPERIMENTAL MODEL AND SUBJECT DETAILS

Cell lines

HEK 293T cell line, B16-F10 cell line and RAW 264.7 cell line are available in our lab (Zhejiang University, College of Pharmaceutical Sciences, Hangzhou, China). The primary hepatocytes were isolated from four-to six-week-old male C57/BL6 mice. HEK 293T cell line and RAW 264.7 cell line were cultured in Dulbecco's Eagle Medium with high glucose. B16-F10 cell line was cultured in RPMI 1640 with high glucose and primary hepatocytes were cultured in William E medium. All of the above medium was supplemented with 10% fetal bovine serum, 100 U/ml penicillin and 100 μg/mL streptomycin. Meanwhile, the Myco-Zero Mycoplasma Removal Agent (Beyotime, C0280S) was added to avoid mycoplasma contamination. These cell lines were grown at 37°C with 5% CO_2.

Animals

The four-to six-week-old male C57/BL6 mice animal models used in our work were commercially obtained from Hangzhou hangsi Biotechnology Co. , Ltd. (Hangzhou, China) at least one week prior to experiments. They were housed in pathogen-free facilities on a 12-h light–dark cycle. All of the animal work was performed under the guidelines of the Laboratory Animal welfare and Ethics Committee of Zhejiang University.

METHOD DETAILS

Construction of functional plasmids

NBS-CRISPR vector

The NBS oligo shown in Table S1 was synthesized by Hangzhou Youkang Biotechnology Co., Ltd. The annealing procedure was as follows: 37°C, 30 min; 95°C, 5 min; 95°C, 1 min for 15 cycles; 25°C, 1 min. The oligo was then cloned into CMV-Cas9-P2A-GFP-P2A-luciferase-pA (Addgene #48138) in our laboratory by replacing the CMV promoter using Hind III and SalI restriction sites. The sgRNAs used in this study were designed online (CHOPCHOP (uib.no)), and the sequences are shown in Table S1.

The NBS-P65-CRISPR vector

The NBS-P65-CRISPR plasmid was constructed by seamless cloning of the linker (3×GGGGS), mCherry and P65 from the pCMV-mCherry-p65 plasmid (Beyotime, D2821) into the NBS-CRISPR vector through PaeI and XbaI restriction sites using the Seamless Cloning Kit (Beyotime, D7010S).

The AAV9-NBS-CRISPR vector

The AAV9-NBS-CRISPR vector was based on the AAV9 vector. Due to the limited gene load capacity, we divided it into two parts, one expressing Cas9 promoted with NBS and the other containing U6 - sgRNA. For subsequent *in vivo* imaging, we inserted the *Renilla* luciferase gene driven by NBS into these two parts.

Cell culture

Isolation and culture of primary hepatocytes

Primary hepatocytes isolation from mouse livers was performed according to the classical two-step collagenase perfusion manual. Briefly, mice were perfused with HBSS without Ca2+, Mg2+, and phenol red until

the liver became gray. Then, the perfusion was switched to collagenase, a type II solution, and the liver was fully digested until it became soft. The soft liver tissue was placed in a 15-mm sterile dish with William E medium, the excess tissue (e.g., lobular capsule membranes, connective and vascular tissue) was removed, and the liver was dissected. The suspension was filtered through a 70-μm cell strainer into a fresh 50 mL tube. The tube was centrifuged at 500 rpm for 5minat 4°C. After resuspending the hepatocytes pellet with 10 mL of William E medium, 20 mL of 50% Percoll solution was added, and the mixture was centrifuged at 1500 rpm for 8minat 4°C. The supernatant was discarded, and the hepatocytes were washed twice with 10 mL of William E medium and centrifuged at 1500 rpm for 8minat 4°C. The washed hepatocytes were re-suspended in 20 mL William E medium supplemented with 10% fetal bovine serum, 100 U/ml penicillin and 100 μg/mL streptomycin. Cells were seeded at a concentration of 5×10^5 cells in 6-well plates and incubated at 37°C in 5% CO_2 for 4–6 h. The cells were washed once in PBS to remove dead cells. Then, the cells were cultured for subsequent use.

HEK293T cells and RAW 264.7 cells

These cells were cultured in high-glucose Dulbecco's Modified Eagle's Medium supplemented with 10% fetal bovine serum and 1× penicillin–streptomycin at 37°C with 5% CO2.

Cell transfection

RAW 264.7 cells

Twenty-four hours prior to transfection, RAW 264.7 cells were seeded into 12-well plates at a density of 2×10^5 cells in complete culture medium. Before transfection, the medium was replaced with fresh complete culture medium, and 100× stock solution of NATE™ was added for a final concentration of 1×. Then, the plate was swirled to distribute the cell population thoroughly and incubated for a minimum of 30 min under normal cell culture conditions. The gene transfer method was performed using lip8000™ Transfection Reagent (Beyotime, C0533) according to the manufacturer's instructions. Then, the cells were incubated at 37°C with 5% CO2 conditions for 24 h to allow gene expression.

HEK 293T cells

Twenty-four hours prior to transfection, HEK 293T cells were seeded into 12-well plates at a density of 2×10^5 in complete culture medium. Before transfection, the medium was replaced with fresh complete culture medium, and the gene transfer was conducted following the Lipofectamine 8000™ Transfection Reagent (Beyotime, C0533) manufacturer's instructions. Then, the cells were incubated at 37°C with 5% CO_2 for 24 h to allow gene expression.

Primary hepatocytes

Transfection was conducted according to the Lipofectamine 3000 Reagent protocol. Briefly, when hepatocytes reached 70%–90% confluence, the plasmid DNA–lipid complex was prepared according to the recommended 2 doses of lipids and incubated for 20minat 37°C. After washing the cells with PBS, the described complex was added to cells cultured in William E medium supplemented with 10% fetal bovine serum. Hepatocytes were incubated for 24hat 37°C. Then, transfected cells were analyzed.

Inflammation stimulation

After transfection for 24 h, LPS (1 μg/mL for RAW 264.7 cells and 10 μg/mL for primary hepatocytes) or TNF-α (50 μg/mL for HEK 293T cells) was added to the medium. For disruption of the NF-κB pathway, HEK 293T cells were incubated for another 12 h with the inhibitor SN50 (working concentration of 18 μM) before stimulation. At 24 h and 48 h post stimulation, cells and supernatants were collected and assayed.

Gene editing assay

The treated cells were collected and harvested to extract genomic DNA with a FastPure Cell/Tissue DNA Isolation Mini Kit (DC102-01, vazyme). PCR amplified the target site from the genomic DNA (primer sequences used are shown in Table S1) and the products were purified with a FastPure Gel DNA Extraction Mini Kit (DC301, vazyme). A T7EI assay was then performed to measure the gene indel rate. Deep sequencing was further performed to assay detailed mutations in edited cells and tissue.

T7EI assay

A total of 200 ng purified PCR products were used as a template for denaturation/reannealing using T7 Endonuclease I Buffer (#M0302S, NEW ENGLAND BioLabs) according to the following program: 95°C, 5 min; 95°C, 1 s, 6 cycles; 85°C, 1 s, 601 cycles; 4°C, indefinitely. After the denature/reannealing step, T7 Endonuclease I was added and the reaction mixture was incubated for 30minat 37°C. After treatment with T7E1, DNA mixtures were loaded on 2% agarose gel electrophoresis and imaged with a gel documentation system (c150, Azure Biosystems, USA). The undigested and digested bands of the grayscale image were calculated by ImageJ. Indel efficiency was calculated with the formula $\{ 1-[1-(b + c)/(a + b + c)]^{1/2} \} \times 100\%$ (a: undigested band intensity; b and c: digested band intensity).

Real-time PCR (qPCR)

PCR amplification of cDNA was performed using Hieff qPCR SYBR Green Master Mix (Low Rox) (11202ES03/08/60, YEASEN) according to the manufacturer's protocol. The procedure was conducted using a QuantStudio Real-Time PCR (QPCR) Detection system as follows: hold stage at 95°C for 5 min, PCR stage 30 cycles of denaturation at 95°C for 10 s and extension at 60°C for 30 s. Gene expression was quantified using the $2^{-\Delta\Delta}$Ct method and normalized to the reference gene β-actin. The primers used for qPCR are shown in Table S1.

Western blotting

Total protein was extracted using RIPA lysis buffer and quantified using a BCA assay. The lysates were mixed with 5X loading buffer boiled for 10minat 100°C. Then, extracted protein samples (20 μg/sample) were separated by 10% SDS-PAGE and transferred onto polyvinylidene difluoride (PVDF) membranes. Membranes were blocked for 1hat room temperature with 5% non-fat milk, followed by incubation overnight at 4°C with following primary antibodies: CRISPR (1:1000, Beyotime),FLAG Tag (1:1000, Affinity), MyD88 (1:1000, Cell Signaling Technology), P65 (1:1000, Proteintech), IκBα (1:20000, Proteintech), phospho-IκBα (1:1000, Affinity), and GAPDH (1:50000, Proteintech). Then, the membrane was further incubated for 2 h with peroxidase-conjugated goat anti-mouse IgG (H + L) (1:50000, Proteintech) and peroxidase-conjugated goat anti-rabbit IgG (H + L) (1:50000, Proteintech). The target proteins were scanned using an enhanced chemiluminescence (ECL) system.

Enzyme-linked immunosorbent assay (ELISA)

Secreted TNF-α and IL-6 protein levels were determined by ELISA kits (KE10002 and KE10007, Proteintech) according to the manufacturer's protocol. Briefly, the collected supernatants were diluted to predetermined concentrations and add to each empty well coated with coating solution and incubated for 2hat 37°C. After discarding the diluted supernatants, the plates were washed with 1× Wash Buffer 4 times, and the detection antibody solution was added. The plates were again washed with 1× wash buffer 4 times after 1 h of incubation at 37°C. HRP-conjugated antibody solution was added and incubated for 40minat 37°C. Then, the plates were washed with 1× wash buffer 4 times, and TMB solution was finally added and incubated at 37°C in the dark for 20–30 min. After the stop solution was added to the plate to stop the reaction, the absorbance of each well was immediately measured at 450 nm in 5 min.

Luciferase assay

After treatment of primary hepatocytes, the cells were collected and lysed with a Firefly Luciferase Reporter Gene Assay Kit (RG005, Beyotime), and the luminescence of the extracted samples was detected with a GloMax 20/20 (Promega, USA).

Animal experiments

Four-to six-week-old C57/BL6 mice were purchased from the Hangzhou hangsi Biotechnology Co. , Ltd. (Hangzhou, China) and housed in pathogen-free facilities on a 12-h light–dark cycle. All of the animal work was performed under the guidelines of the Laboratory Animal welfare and Ethics Committee of Zhejiang University.

Two hundred microliters of AAV9 mixture (5×10^{11} genome copies of AAV9-Cas9 and 1×10^{12}genome copies of AAV9-sgRNA) dilluted in sterile phosphate buffered saline was delivered to C57/BL6 mice intravenously via lateral tail vein injection. *In vivo* imaging system (IVIS) was performed 30min after 100 ng/mice D-luciferase postassium salt was administrated via intraperitoneal injection.

Inclusion and exclusion criteria

No inclusion and exclusion criteria were applied to the data collection or the subject selection in this study.

QUANTIFICATION AND STATISTICAL ANALYSIS

All experiments were independently repeated at least three times. Results are shown as means ± SEM. All statistical data analyses were performed using GraphPad PRISM version 9.0.0. The one-way ANOVA was subjected for multiple-group with one factor comparisons, the two-way ANOVA was subjected for multiple-group with two factors comparisons and the unpaired t-test was performed for two unpaired groups.